Conf-810831--99

CONF-810831--99

DE83 007654

To be submitted to J. Nucl. Mater. (1981).

DEPTH DISTRIBUTION OF 20-keV HELIUM-ION IRRADIATION-INDUCED CAVITIES IN NICKEL*

G. Fenske, S. K. Das and M. Kaminsky

Argonne National Laboratory
Argonne, Illinois 60439, U.S.A.

Transmission electron microscopy has been used to study the effect of total dose on the depth distribution of cavities (voids or bubbles) in nickel irradiated at 500°C with 20-keV $^4He^+$ ions. A transverse sectioning technique allowed us to obtain the entire depth distribution of cavities from a single specimen. The diameter, number density and volume fraction of cavities were measured as a function of depth from micrographs taken from samples sectioned parallel to the direction of the incident beam. The results for the doses at 2.9×10^{15} and 2.9×10^{16} ions/cm^2 show an increase in the average cavity diameter, number density and volume fraction with increasing dose. A further increase in dose from 2.9×10^{16} to 2.9×10^{17} ions/cm^2 also shows an increase in the average cavity diameter but a decrease in the number density. This observation is interpreted as evidence for the coalescence of cavities.

1. INTRODUCTION

Helium blistering can become an important process for surface erosion of first wall components for certain types and operating conditions of fusion reactors [1-4]. In order to develop effective methods to reduce or eliminate this erosion process, a better understanding of the mechanisms leading to blistering and surface exfoliation is desirable. Studies of the depth distribution of dislocations and cavities (voids, bubbles) in helium implanted metals will provide better insights into the basic mechanisms underlying the blistering process. Different blistering models have been proposed of which some invoke the coalescence of bubbles and the build-up of internal gas pressure as a precursor to blister appearance [5-12], while others do not [13-16]. For example, some models of the latter type consider the build-up of integral lateral stresses rather than the build-up of gas pressure in bubbles and bubble coalescence as the main driving force for blister appearance.

In recent studies [12,17] of the depth distribution of gas-filled cavities in nickel implanted at 500°C with 500-keV $^4He^+$ ions at different doses, we obtained direct evidence for the formation of blisters preceded by the nucleation, growth and coalescence of cavities. One goal of the present study is to determine how the cavity size and number density, and the volume swelling change as a function of dose and implant depth for nickel held at 500°C during the implantation with helium at a lower energy of 20-keV. Another goal is a search for evidence for gas bubble coalescence for the irradiation conditions stated. Finally, these studies should help to clear up a reported discrepancy [18] between calculated projected ranges and the thickness of exfoliated blister skins for 20-keV $^4He^+$ irradiations of annealed nickel. We reported earlier [19] that for 20-keV $^4He^+$ irradiations the skin thicknesses were about twice the calculated average projected ranges using Brice's computer codes [20] together with LSS electronic stopping and Thomas-Fermi nuclear stopping powers.

2. EXPERIMENTAL TECHNIQUE

High-purity (99.995%) polycrystalline nickel foils obtained from the Materials Research Corporation were used in the experiments. They were metallographically polished, then annealed at 900°C for two hours in a vacuum of $\sim 2.7 \times 10^{-5}$ Pa, and finally electropolished prior to implanting them with helium ions. The foils were irradiated at 500°C in a vacuum of $\sim 10^{-5}$ Pa with a mass-analyzed beam of 20-keV helium ions to doses of 2.9×10^{15}, 2.9×10^{16} and 2.9×10^{17} ions/cm^2. Following implantation, the foils were first lightly sputter-cleaned with 2-keV Ar^+ ions, then given a nickel strike and finally electroplated with nickel. The electroplated samples were then sectioned parallel to the direction of the incident beam. Thin foils suitable for TEM were prepared by electrolytic jet polishing of 3-mm discs spark cut from the sectioned samples. This transverse sectioning technique, whose details are described elsewhere [21], permitted us to study the entire depth distribution of bubbles from a single section. Similar techniques have been used to study the depth distribution of damage [22] and voids [23-25] but with the exception of our recent paper [19], no quantitative data has been reported for 20-keV $^4He^+$ implanted nickel. Transmission electron micrographs of the cavities in the implanted region were analyzed to determine the average cavity diameter, number density and volume swelling as a function of depth from the implanted foil surface using a Zeiss particle size analyzer.

3. RESULTS

Figures 1a-c show bright field micrographs of the cavity microstructure as a function of depth

for nickel foils implanted to doses of 2.9 x 10^{15}, 2.9 x 10^{16} and 2.9 x 10^{17} ^{4}He ions/cm^2.

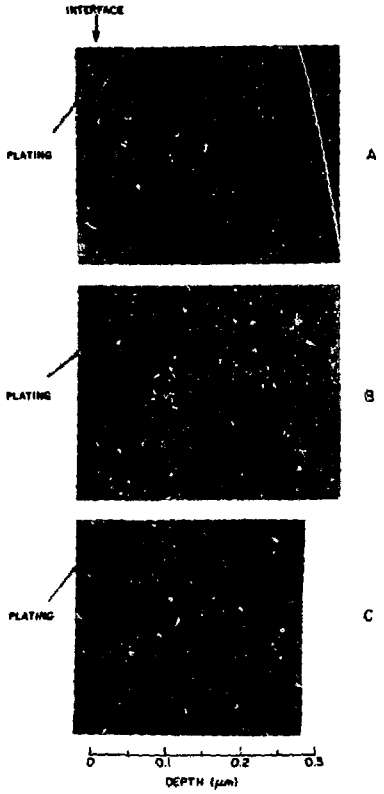

FIG. 1. The depth distribution of the cavity microstructure of nickel irradiated with 20-keV $^4He^+$ ions at 500°C to doses of (a) 2.9 x 10^{15} ions/cm^2, (b) 2.9 x 10^{16} ions/cm^2 and (c) 2.9 x 10^{17} ions/cm^2.

The interface between the implanted foil and the nickel plating (Wood's strike) is clearly seen. The cavities observed in the plating are believed to be hydrogen-filled bubbles generated and subsequently trapped in the matrix when the nickel strike was applied. We have shown earlier [21] that the cavities in the strike do not affect the radiation-induced cavity microstructure in the implanted foil. At 2.9 x 10^{15} and 2.9 x 10^{16} ions/cm^2, a large fraction of the cavities appear to have been preferentially nucleated at dislocations (Figs. 1a and 1b). This behavior is similar to that observed for 500-keV implantations at similar peak helium concentrations [17]. At 2.9 x 10^{17} ions/cm^2, the size and density of cavities are too high to observe preferential siting.

Quantitative data on the average cavity size, density and volume swelling as functions of the implant depth are shown in Figs. 2a-c. Figure 2d shows the energy deposition (for atom displacement) and projected range profiles for 20-keV ^{4}He ions in nickel calculated with three methods: A Monte Carlo technique using Biersack's TRIM code [26], an Edgeworth expansion using Winterbon's spatial moments [27] and Brice's code [20] which assumes a Gaussian range distribution. The profiles based on Brice's code and Winterbon's moments used theoretical LSS electronic stopping and a Thomas-Fermi nuclear screening function. Biersack's TRIM calculations are based on theoretical LSS electronic stopping and a Moliere nuclear screening function.

At a dose of 2.9 x 10^{15} ions/cm^2 the average cavity diameter was ≈30 Å and was independent of depth. The maximum cavity density, ≈5 x 10^{16}/cm^3 occurred in the depth interval between 0.10 and 0.12μm. Beyond ≈0.3μm, the density decreased to near-zero values. The maximum volume swelling at 2.9 x 10^{15} ions/cm^2 (∿0.13%) also occurred between 0.10 and 0.12μm.

At 2.9 x 10^{16} ions/cm^2, the cavity size exhibited a slight depth dependence as seen in Fig. 2b. The location of the maximum average values for the diameter, density and volume swelling occurred between ∿0.07 and 0.10μm. The maximum density increased to ∿2 x 10^{17}/cm^3, and the peak volume swelling was ∿0.8%. Beyond ∿0.25μm, the density and volume swelling decreased to zero.

Figure 2c indicates that at 2.9 x 10^{17} ions/cm^2 the cavities near the interface were ∿60 Å in diameter, while further in they increased to ∿120 Å, and then decreased to ∿40 Å between 0.17 and 0.23μm. Beyond ∿0.23μm, the density is practically zero, although a few small cavities were observed beyond this depth. The maximum swelling (∿14%) occurred between 0.10 and 0.13μm while the maximum number density occurred between 0.10 and 0.18μm.

In comparing Figs. 2a-c with 2d, one notes that the maximum volume swelling occurs at a depth significantly larger than the most probable projected range and the maximum in the energy deposition profile based on the Gaussian distribution. However, better agreement between the most probable range and the location of the maximum volume swelling is obtained using the Edgeworth expansion or the TRIM code for the calculation of the range distribution.

4. DISCUSSION

The results presented above, together with our previous data [12,17,19] for 20- and 500-keV implantations of nickel provide detailed information on the mechanisms involved in blistering. For example, the information on the depth profiles can be compared with theoretical projected ranges and blister skin measurements. Secondly, the quantitative data on the cavity size, density and volume swelling can be used to determine if sufficient helium is present to exceed the strength of the load-supporting cross-section in the peak swelling region.

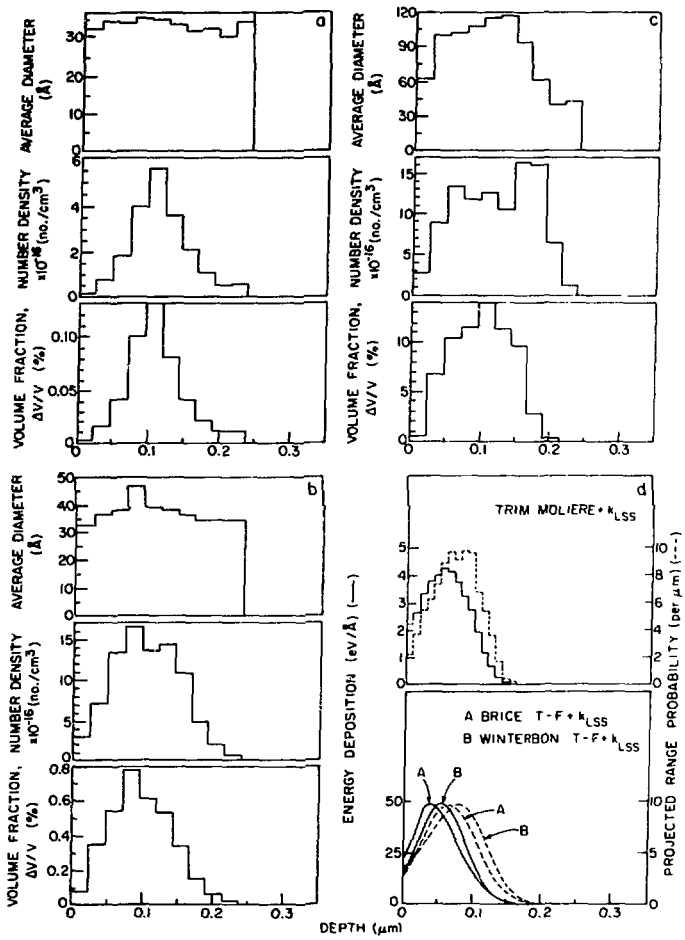

FIG. 2. The average diameter, number density and volume fraction of cavities as a function of depth in nickel implanted at 500°C with 20-keV $^4He^+$ ions to doses of (a) 2.9 x 10^{15} ions/cm^2, (b) 2.9 x 10^{16} ions/cm^2 and (c) 2.9 x 10^{17} ions/cm^2. Figure 2(d) shows the calculated depth distribution of the projected range (dashed curves) and the energy deposited into damage (solid curves) according to Biersack (see TRIM) [26], Winterbon (see B) [27] and Brice (see A) [20].

The discrepancy between the calculated range profiles in Fig. 2d and the measured volume swelling distribution in Fig. 2c has been discussed in greater detail elsewhere [19]. The difference between the Gaussian range distribution and the Edgeworth or Monte Carlo profiles is a result of the higher-order moments (i.e. skewness and kurtosis) which are incorporated in the Edgeworth and Monte Carlo calculations but not in the Gaussian profile. As a result, the Gaussian approximation underestimates the most probable projected range for this particular energy and projectile-target combination. While improved agreement is obtained with the Edgeworth and Monte Carlo profiles, a discrepancy still exists between the location of the maximum volume swelling at 2.9 x 10^{17} ions/cm^2 and the calculated most probable range based on the Edgeworth or Monte Carlo distributions in Fig. 2d. This discrepancy has been attributed [19] to inaccurate data on the electronic stopping power for this energy range, and to the neglect of the influence of volume swelling on the calculation of the range and energy deposition profiles.

The reported discrepancies [18] between calculated blister skin thickness based on coalescence models and measured skin thickness can be accounted for when the three factors mentioned above are considered. Table I compares measured skin thickness with calculated ones based on models which use bubble coalescence or integrated lateral stresses as the dominant mechanisms for blister formation. The coalescence models predict that the blister skin separates at the most probable projected range whereas integrated lateral stress models predict that separation occurs either at the location of the maximum gradient in the shear stresses or at the location of the maximum integrated lateral stress. By assuming that the stresses are proportional to the volume swelling (prop. to He concentration), the lateral stress models predict skin thicknesses equal to $\langle R_p \rangle + \Delta R_p$ (ΔR_p is the range straggling) or the end of the range profile for a Gaussian range profile. Table I shows predicted skin thicknesses based on the experimental swelling profiles. It is seen that the skin thicknesses predicted by coalescence models agree well with the measured values.

TABLE I. Comparison of Measured and Predicted Skin Thickness

	20 keV	500 keV
Predicted Skin Thickness (μm) (Based on the Measured Volume Swelling Profiles)		
- Coalescence	0.11-0.14[a]	1.10-1.15[b]
- Integrated Lateral Stress	0.24-0.28[c]	1.4-1.5[d]
Measured Skin Thickness (μm)	0.10-0.16	1.05-1.15

a) Taken from the data for the 500°C irradiation to dose of 2.9×10^{17} ions/cm^2. The effect of volume swelling was extrapolated to the critical blister formation dose of $4\text{-}5 \times 10^{17}$ ions/cm^2. Also includes the correction for the material lost during the Ar-sputter cleaning process.

b) Taken from the data for the 500°C irradiation to 1×10^{18} ions/cm^2. Includes the correction for the Ar-sputter cleaning process.

c) Interval where the volume swelling profile ends at 2.9×10^{16} ions/cm^2, extrapolated to the critical blister formation dose of $4\text{-}5 \times 10^{17}$ ions/cm^2.

d) Interval where the volume swelling ends at 5×10^{16} ions/cm^2.

Figure 3 shows the average cavity diameter, number density and volume swelling at the maximum-swelling depths as functions of the total implant dose for nickel implanted with 20-keV $^4He^+$ ions at 500°C. As the dose is increased from 2.9×10^{15} ions/cm^2 to 2.9×10^{16} ions/cm^2 the cavity size, number density and swelling increase with increasing dose. However, upon further increase to 2.9×10^{17} ions/cm^2 one notices a marked increase in average cavity size and in the volume fraction but a decrease in the number density. We interpret this as evidence for bubble coalescence. While the critical dose for blister formation under these conditions is $\sim 4\text{-}5 \times 10^{17}$ ions/cm^2, coalescence at the maximum volume swelling depth is already occurring at a dose between 2.9×10^{16} and 2.9×10^{17} ions/cm^2. In order to illustrate how bubble coalescence influences the formation of blisters, one needs to examine the tensile stresses acting on the load-supporting cross section of the implanted region. The load-supporting cross section is defined as an area of bulk metal (excluding the area occupied by the cavities) parallel to the irradiated surface located at the depth of maximum swelling. Through this examination it can be demonstrated that a sufficient quantity of helium is available in the implanted region to generate the pressures required to fracture the load-supporting cross section that has been reduced by coalescence.

An analysis of this type which was similar to the blistering model based on bubble coalescence presented by Evans [10] has been presented elsewhere for 500-keV helium implantation of nickel at 500°C. It can be shown that the gas pressure, p, inside a cavity of radius, r

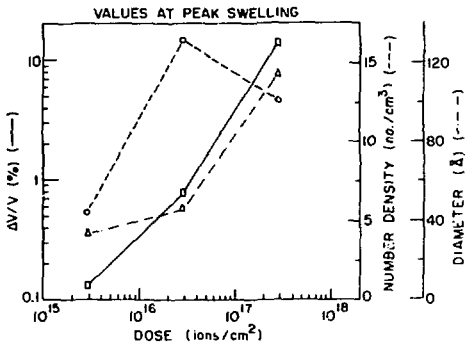

FIG. 3. The average cavity diameter, the cavity number density and the volume swelling at the maximum swelling depth for nickel implanted with 20-keV $^4He^+$ ions at 500°C to doses ranging from 2.9×10^{15} to 2.9×10^{17} ions/cm^2.

required to exceed the strength, σ, of the matrix between the cavities can be given as:

$$p \geq \sigma[(\pi r^2 c 2/3)^{-1} - 1] + \frac{2\gamma}{r} \qquad (1)$$

where γ is the surface energy and c is the cavity density.

If the strength, σ, is replaced with either the fracture strength ($\sim 1.4 \times 10^{10}$ dynes/cm^2) [28], or the true stress at maximum load ($\sim 2 \times 10^9$ dynes/cm^2) the gas pressure determined with Eq. (1) is that required to fracture or initiate "continued necking" of the load-supporting columns, respectively. If we assume a surface energy of 1000 ergs/cm^2 and use the data at the peak-swelling depth for the 20-keV 500°C irradiation to a dose of 2.9×10^{17} ions/cm^2, the gas pressures required for fracture and necking are 4.3×10^{10} dynes/cm^2 and 9.1×10^9 dynes/cm^2, respectively. To generate a pressure of 4.3×10^{10} dynes/cm^2 a density of approximately 7.6×10^{22} He atoms/cm^3 is required, assuming Rowlinson's [29] expression for the equation of state for helium. The calculated peak helium concentration for 20-keV He ions at 2.9×10^{17} ions/cm^2 is $\sim 2.8 \times 10^{22}$ ions/cm^3; thus, if all of the helium in the matrix surrounding the cavity was contained in the cavity, the density (in the cavity) would be 2.8×10^{23} atoms/cm^3. Therefore, only ≈30% of the helium contained in the matrix is required to obtain a pressure high enough to exceed the fracture strength.

5. CONCLUSION

The depth distributions of radiation-induced cavities were measured in nickel foils implanted with 20-keV $^4He^+$ ions. The results indicate that the peak volume swelling occurs at a depth larger than the calculated most probable projected range, which has been attributed to uncertainties in the electronic stopping used to calculate the range profile, variations in the

target density due to radiation induced volume swelling and differences in the methods used to calculate the range profiles. When appropriate corrections for the electronic stopping and the radiation induced volume swelling are made, blister formation models based on bubble coalescence accurately predict blister skin thicknesses at low energies. Data on the cavity density in the depth interval where the maximum volume swelling occurs, indicates that beyond a certain dose, 2.9 x 10^{16} ions/cm^2, for 20-keV implantations in nickel held at 500°C, the cavity density decreases with further increases in the dose. This trend is a result of cavity coalescence and is similar to that observed at 500°C for 500-keV ^{4}He implantations of nickel for doses above 1 x 10^{17} ions/cm^2. As such, this observation supports the coalescence model of blister formation. Furthermore, a calculation of the quantity of helium required to fracture the load-bearing matrix between coplanar cavities demonstrates that a sufficient quantity of helium is present to generate the required gas pressures.

REFERENCES

[1] M. Kaminsky, IEEE Trans. Nucl. Sci., NS-18 203 (1971).
[2] M. Kaminsky, CRC Critical Reviews in Solid State Sciences, 6 (1976) 433.
[3] S. K. Das and M. Kaminsky, Advances in Chemistry, Volume 158 (Ed. M. Kaminsky), 112, 1976.
[4] John Gittus, Irradiation Effects in Crystalline Solids, Applied Science Publishers LTD, London, 1978, Chapter 10, page 484ff.
[5] M. Kaminsky, Adv. Mass Spectr. 3 (1964) 69.
[6] W. Primak and J. Luthra, J. Appl. Phys., 37 (1966) 2287.
[7] R. S. Blewer and J. Maurin, J. Nucl. Mater. 44 (1972) 260.
[8] S. K. Das and M. Kaminsky, J. Appl. Phys. 44 (1973) 25.
[9] G. M. McCracken, Japan J. Appl. Phys. Suppl. 2, Part 1 (1974) 269.
[10] J. H. Evans, J. Nucl. Mater. 61 (1976) 1.
[11] O. Auciello, Rad. Effects 30 (1976) 11.
[12] G. Fenske, S. K. Das, M. Kaminsky and G. Miley, Nucl. Instr. and Methods 170 (1980) 465.
[13] R. Behrisch, J. Bøttiger, W. Eckstein, U. Littmark, J. Roth and B. M. U. Scherzer, Appl. Phys. Lett. 27 (1975) 189.
[14] J. Roth, in Applications of Ion Beams to Materials, Eds. G. Carter, J. S. Colligon and W. A. Grant (Inst. of Physics, London) 1976, 280.
[15] M. Risch, J. Roth and B. M. U. Scherzer, in Plasma-Wall Interactions (Pergamon Press, New York) 1977, 391.
[16] E. P. Eernisse and S. T. Picraus, J. Appl. Phys. 48 (1977) 9.
[17] G. Fenske, S. K. Das and M. Kaminsky, J. Nucl. Mater. 85 & 86 (1979) 707.
[18] S. K. Das, M. Kaminsky and G. Fenske, J. Nucl. Mater. 76 & 77 (1978) 215.
[19] G. Fenske, S. K. Das, M. Kaminsky, G. Miley, B. Terreault, G. Able and J. P. Labrie, J. Appl. Phys. 52 (1981) 3618.
[20] D. K. Brice, Ion Implantation Range and Energy Deposition Codes: COREL, RASE4 and DAMG2; Sand 75-0622 (1977).
[21] G. Fenske, S. K. Das and M. Kaminsky, J. Nucl. Mater. 80 (1979) 373.
[22] J. Narayan, D. S. Oen and T. S. Noggle, J. Nucl. Mater. 71 (1977) 160.
[23] R. A. Spurling and C. G. Rhodes, J. Nucl. Mater. 44 (1972) 341.
[24] J. B. Whitley, G. L. Kulcinski, P. Wilkes and J. Billen, J. Nucl. Mater. 85 & 86 (1979) 701.
[25] C. H. Henager, J. L. Brimhall, and E. P. Simonen, Rad. Eff. 36 (1978) 49.
[26] J. P. Biersack and L. G. Haggmark, Nucl. Instr. and Methods 174 (1980) 257.
[27] K. B. Winterbon, Ion Implantation Range and Energy Deposition Distributions, Vol. 2, Low Incident Ion Energies (Plenum Press, New York) 1975.
[28] W. D. Jenkins and T. G. Diggs, J. Res. Natl. Bur. Stand. 48 No. 4 (1952) 313.
[29] J. S. Rowlinson, Mol. Phys. 7 (1963/64) 349.

*Work supported by the U. S. Department of Energy under Contract W-31-109-Eng-38.

DISCLAIMER